J Mater Sci: Mater Electron (2021) 32:16544–16553

Impact of ZrO_2 additive on the microstructure, magnetic properties, and temperature dependence of the initial permeability of LiTiZn ferrite ceramics

A. V. Malyshev[1,*], A. B. Petrova[1], and A. P. Surzhikov[1]

[1] *Tomsk Polytechnic University, Lenina Avenue 30, 634050 Tomsk, Russia*

Received: 8 February 2021
Accepted: 16 May 2021
Published online: 31 May 2021

ABSTRACT

The effect of the diamagnetic ZrO_2 addition on the microstructure and magnetic properties of LiTiZn ferrite ceramics, including the shape and parameters of the temperature dependence of the initial permeability, has been investigated. The defect structure of ferrite ceramic samples is assessed according to our earlier proposed method based on the mathematical treatment of the experimental temperature dependencies of the initial permeability. It was found that the defect structure of ferrite ceramics increased by 350% with an increase in the concentration of the ZrO_2 additive in the range of (0–0.5) wt.%. In this case, for the same samples, the increase in the true physical broadening of diffraction peaks is only 20%, and the coercive force by 50%. Simultaneously, the maximum of the experimental temperature dependence of the initial permeability dropped by 45%. The microstructure of all samples is characterized with a similar average grain size according to the SEM data. However, samples with 0.5 wt.% of ZrO_2 are characterized by the formation of conglomerates. A linear relationship was obtained between the defect structure and the width of the diffraction peaks, which indicates that this parameter is related to the elastic stress of ferrite ceramics. These results suggest that the high sensitive proposed method can be recommended for impurity and defect monitoring of soft ferrite products.

1 Introduction

LiTiZn ferrite ceramics are widely used in microwave devices due to their low cost and excellent ferromagnetic properties with high values of saturation magnetization and Curie point. Such materials have low microwave dielectric loss. Due to the successful combination of electromagnetic properties, such ceramics are used in the production of such microwave devices as phase shifters, isolators, and microwave absorbers.

Defects in the crystal structure of ferrite materials largely determine the properties of ferrite products obtained by various production methods. It is the

Address correspondence to E-mail: malyshev@tpu.ru

https://doi.org/10.1007/s10854-021-06210-z

manufacturing stage that determines, in the main, the defect structure of various ferrite products. Consequently, the development of modes for ferrite production with the possibility of varying both the chemical composition and the defect structure of the material is an urgent problem of ferrite material science.

Lithium ferrites are usually obtained by the ceramic method of double sintering, where in the first stage, solid-state reactions are carried out between oxides and/or carbonates followed by high-temperature sintering in the second stage [1–3].

Defect structure of ferrite ceramics includes intragranular defects of the conjugation of grain boundaries and crystal lattice defects. Various types of defects and phase inclusions (including diamagnetic impurities) appear when sintering ferrite ceramics using ceramic technology [4–6]. It is obvious that such defects, along with intragranular porosity, inhibit the domain walls and, ultimately, worsen the electromagnetic properties of ferrite ceramics. The latter is determined not only by the chemical composition of the material but also by the content and distribution of defects in it. Thus, it is important to know the relationship between defects and magnetic properties in the production of ferrite materials.

The diamagnetic additive ZrO_2 is used in this work not for improving the electromagnetic properties, but to test the previously proposed method for calculating the defect structure of ferrite ceramics based on the mathematical analysis of the experimental temperature dependence of the initial permeability μ_i. This method has shown its relatively high sensitivity in comparison with the known magnetic methods, as well as XRD [7].

The novelty of the study lies in the relationship between the low concentrations of the ZrO_2 additive and the form of the temperature dependence of the initial permeability of LiTiZn ferrite ceramics and its defect structure. Also, the influence of ZrO_2 diamagnetic additive on the structural and magnetic properties was studied.

2 Experimental

2.1 Materials

The industrial ferrite powder, synthesized by usual ceramic technology from a mechanical mixture of oxides and carbonates in Ferrit-Domen Co., St. Petersburg, Russia, was used to prepare the samples. Mixture composition (wt. %): Li_2CO_3–11.2; TiO_2–18.65; ZnO–7.6; $MnCO_3$–2.74; Fe_2O_3–59.81 [7]. In addition, Bi_2O_3 was used for liquid-phase sintering. The ferrite code is SL-187.

ZrO_2 (chemically pure) was used for diamagnetic additives in the synthesized LiTiZn ferrite for modeling the appearance of additives in the form of various oxides and defects that occur during ferrite products production.

We had explored model ferrite samples without additives (no additives) and samples with ZrO_2 additives of 0.1, 0.25, 0.5 wt.%. Such an additive is often used to modify the electro-physical properties of materials.

Toroidal samples with dimensions 18 × 14 × 2 mm^3 were used for electromagnetic measurements.

Sintering of the samples was carried out in the air under laboratory conditions at a temperature of 1010 °C for 2 h.

The results of thermomagnetometric measurements (Fig. 1) showed that the Curie points ($T_{C\ DTG}$) for samples of LiTiZn ferrite ceramics with 0.75 and 1 wt.% of ZrO_2 differ significantly (on 6–8 degrees) from the Curie points for samples without or containing 0.1, 0.25 or 0.5 wt.% of ZrO_2. Such changes may indicate an alteration in the chemical composition of the ferrite.

We emphasize that ferrite samples with diamagnetic ZrO_2 additive concentrations 0.75 and 1 wt.% were not suitable for the correct comparative study. As a result, the experimental results of this investigation were given only for four types of samples: no additives, with a ZrO_2 additive concentration of 0.1, 0.25 and 0.5 wt. %.

2.2 Characterization techniques

The Curie points ($T_{C\ DTG}$) were determined by the thermomagnetometric method on an STA 449C Jupiter thermal analyzer (Netzsch, Germany) [8]. The TG and DTG curves were obtained in the heating mode at a rate of 50°/min in a constant magnetic field of about 5 Oe.

The hydraulic press PGr-10 was used for compaction of toroidal samples [7].

The Retsch Emax ball mill was used for homogeneous mixing of the diamagnetic additive ZrO_2 in ferrite samples.

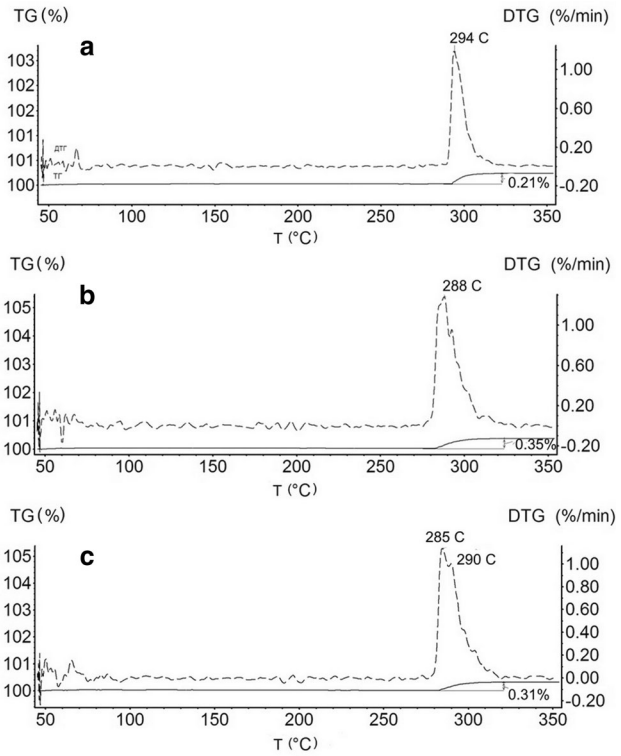

Fig. 1 TG and DTG curves obtained for LiTiZn ferrite ceramic samples: **a** no additives; **b** 0.75% of ZrO_2; **c** 1% of ZrO_2

The diffractograms were obtained using an ARL X'TRA X-ray diffractometer, Cukα radiation. Scanning angle 2θ = (10–80) degrees with a scan rate of 0.01°/s. The phase compositions of the examined samples were determined using the PDF-4 powder database of the International Centre for Diffraction Data (ICDD). PDF card 04-020-6937. The XRD patterns were processed by the full-profile Rietveld analysis using the Powder Cell 2.5 software.

Williamson-Hall's formula [9]

$$\beta^2 = \{\lambda/[D_c \cdot cos(\theta)]\} + [4 \cdot \varepsilon \cdot tg(\theta)]^2, \quad (1)$$

where, β–physical broadening of the diffraction maximum; λ–radiation wavelength; D_c–coherent scattering region (crystallite size); θ–Bragg reflection angle; ε–strain of the crystal lattice.

The parameters of the magnetic hysteresis loop were measured using an oscillographic circuit (based on a Tektronix-2012B two-channel oscilloscope) [7].

Electronic images were obtained with a Hitachi TM-3000 scanning electron microscope on polished and chemically etched transverse cleavages of the samples. The average grain size (D) was calculated by the intercept method.

The technique for measuring inductance using an automatic bridge meter is given in [7, 10]. The measurement was carried out with an E4960AL low-frequency meter in an electromagnetic field with a frequency of 1 kHz and a low strength of 8 A/m.

The initial permeability (μ_i) of the toroidal ferrite samples was calculated by using the formula (2) [5].

$$\mu_i = \frac{L \cdot 10^7}{2 \cdot h \cdot N^2 ln(D/d)}, \quad (2)$$

L–the induction of coil (H); N–number of turns; h–toroid height (m); D/d–toroid outside/inside diameter (m).

3 Results and discussion

3.1 X-ray diffraction analysis

Figure 2 shows the diffractograms for model samples of LiTiZn ferrite ceramics. The scale is the same for both 2θ and intensity.

Table 1 shows that the addition of ZrO_2 has a weak effect on the X-ray structural parameters of the ferrite ceramics. With an increase in the concentration of ZrO_2, the lattice parameter and crystallite size (Coherent scattering regions) slightly decrease. In this case, the microstrain is practically independent of this parameter. Thus, XRD method was not sensitive for determining small concentrations of the ZrO_2 additive up to 0.5 wt.%. Clearly, such behavior can be explained by the sensitivity of X-ray diffractometer, which is determined by the ratio of the absorption coefficients of the determined phase and the mixture.

Emphasize that the nature of the effect of ZrO_2 additive on the X-ray structural parameters differs significantly from the previously discovered effect of Al_2O_3 additive on ferrite ceramics of the same composition [10]. The significant difference in XRD results for LiTiZn ferrite with ZrO_2 and Al_2O_3 additives is possibly caused by the different absorption coefficients of the additives in the mixture.

3.2 Morphological analysis

Figure 3 shows the electron micrographs of LiTiZn ferrite ceramic samples.

The average grain size calculated by the intercept method differs slightly for different model samples D = (7.1 ± 0.4) μm. The samples with the addition of

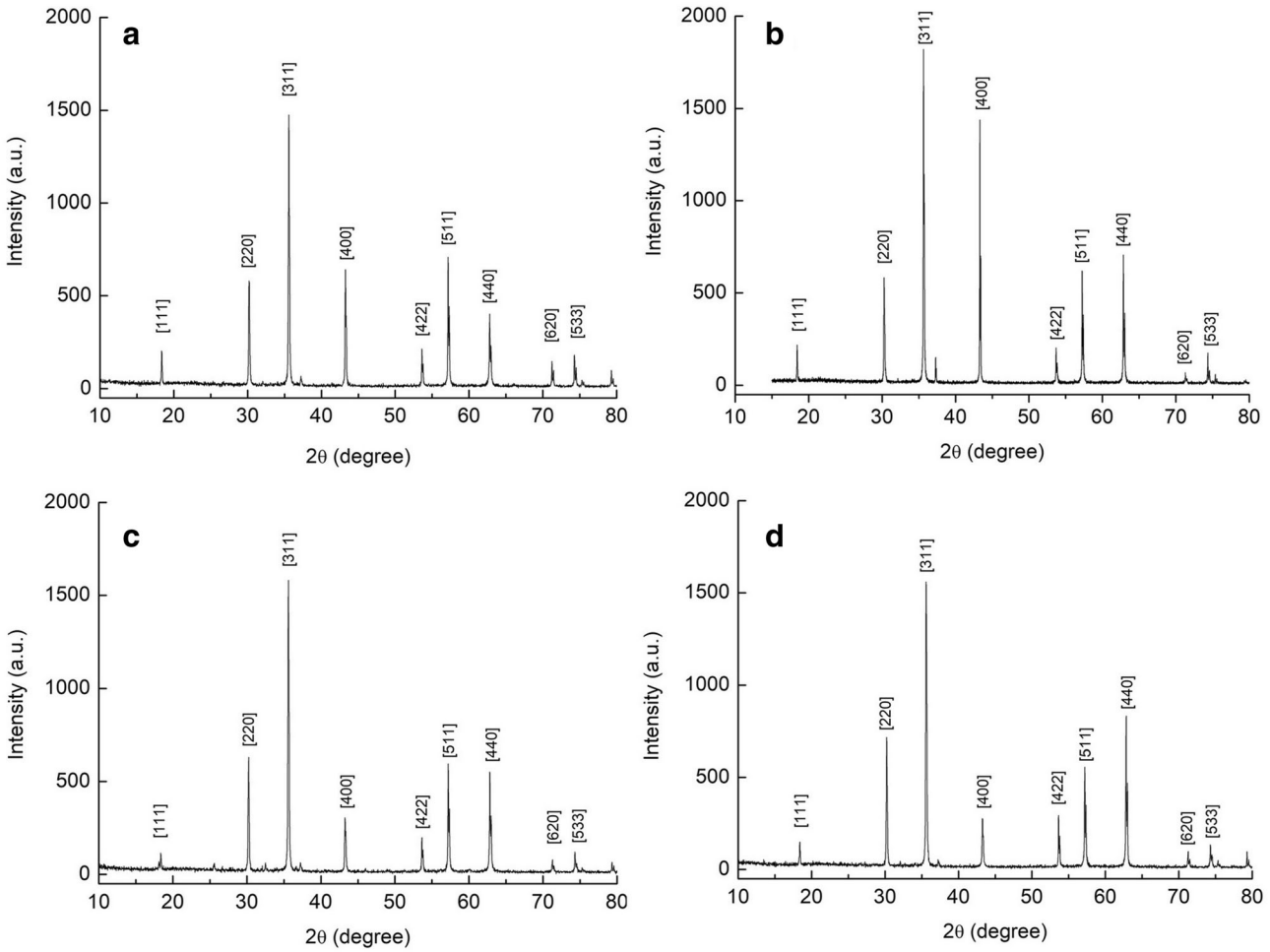

Fig. 2 X-ray diffraction patterns of LiTiZn ferrite samples: **a** no additives; **b** 0.1% of ZrO_2; **c** 0.25% of ZrO_2; **d** 0.5% of ZrO_2

Table 1 Effect of ZrO_2 additive on the X-ray structural parameters of LiTiZn ferrites

Samples type	Lattice parameter (nm)	Micro-strain·10^4	Crystallite size (nm)
No additive	0.8367	4	93
Add. 0.1%	0.8366	4	88
Add. 0.25%	0.8364	5	86
Add. 0.5%	0.8363	5	86

0.5 wt.% ZrO_2 are characterized by the formation of agglomerates. As can be seen from Fig. 3, all samples have a polycrystalline structure with formed grain boundaries. Surely, the white intergranular inclusions correspond to Bi_2O_3 added during the synthesis of industrial ferrite powder. Such behavior can also be caused by ZrO_2 additives.

3.3 Temperature dependencies of the initial permeability

Figure 4 shows the impact of ZrO_2 additive on the temperature dependencies of the initial permeability for LiTiZn ferrite ceramic samples.

The mathematical treatment of the temperature dependencies of initial permeability was carried out using the phenomenological expression (3) proposed in [7]. As a result, the calculated values of the main parameters of the phenomenological expression, including and the Curie point (Tc), and the defect

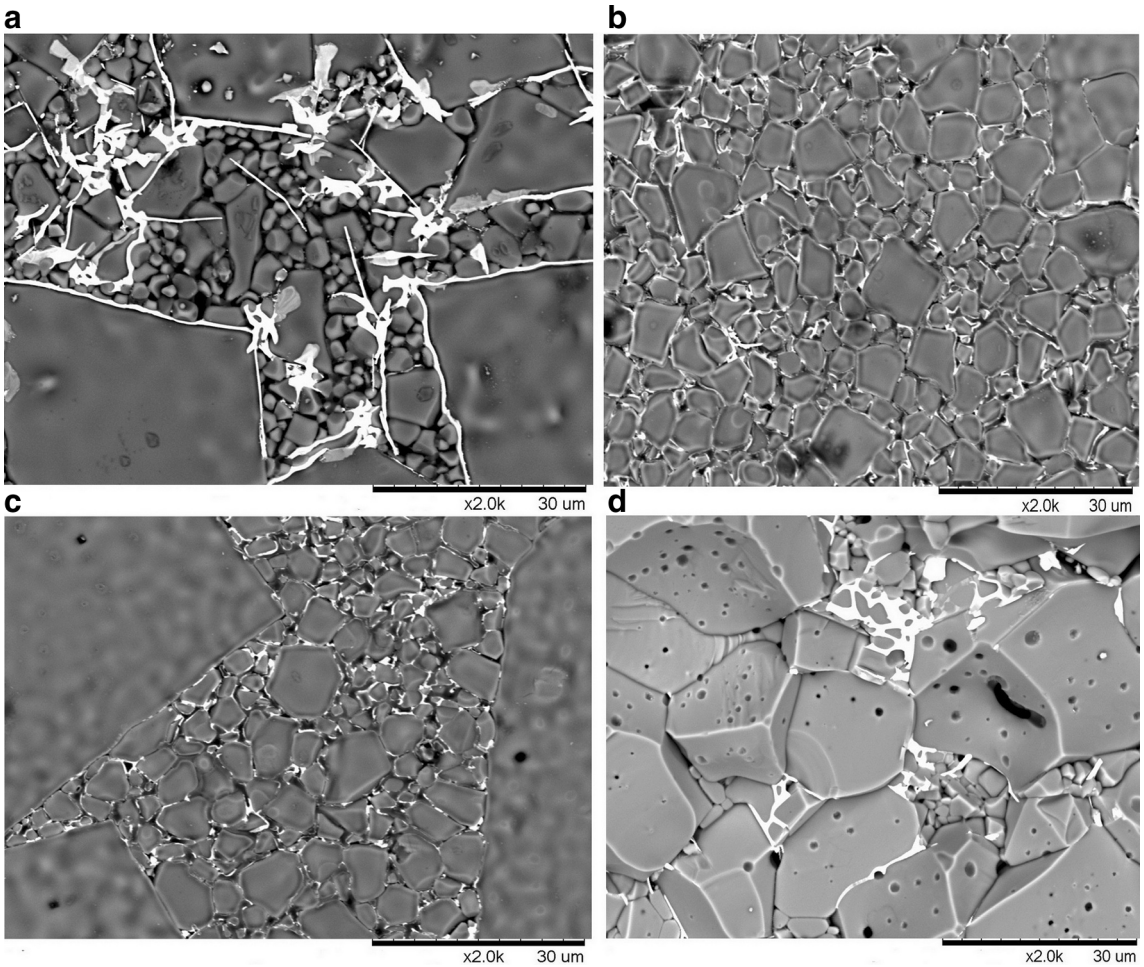

Fig. 3 Electron micrographs of LiTiZn ferrite ceramic samples: **a** no additives; **b** 0.1% of ZrO_2; **c** 0.25% of ZrO_2; **d** 0.5% of ZrO_2

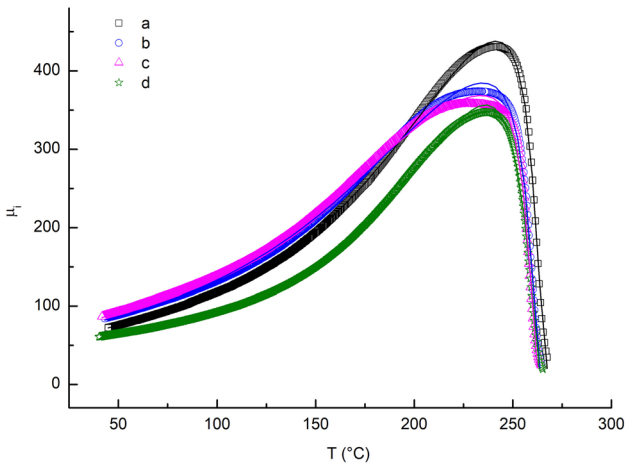

Fig. 4 Temperature dependencies of the initial permeability of LiTiZn ferrite ceramic samples: **a** no additives; **b** 0.1% of ZrO_2; **c** 0.25% of ZrO_2; **d** 0.5% of ZrO_2. Symbols—experimental data, solid lines—calculated curves

structure (β/α) were obtained. Table 2 shows the calculated main parameters of the phenomenological expression, as well as the parameters of the temperature curves.

$$\mu_i = \frac{1+x}{1+N\cdot x}, x = \left[\frac{\left(1-\frac{T}{T_c}\right)^{\delta}}{\alpha\left(1-\frac{T}{T_c}\right)^{\gamma}+\beta}\right]^{g} \tag{3}$$

The coefficientsα, β, γ and δ are determined by the relations (4), (5), (6):

$$\alpha = \frac{K_1(0)}{M_s^r(0)},\ \beta = \frac{\lambda_s(0)}{M_s^r(0)}\cdot\sigma,\ \delta = (r-n)f, \gamma = (m-n)f \tag{4}$$

$$\frac{K_1(T)}{K_1(0)} = \left[\frac{M_s(T)}{M_s(0)}\right]^{m}, \frac{\lambda_s(T)}{\lambda_s(0)} = \left[\frac{M_s(T)}{M_s(0)}\right]^{n} \tag{5}$$

$$M_s(T) = M_s(0)\left[1-\frac{T}{T_c}\right]^{f} \tag{6}$$

Table 2 Impact of ZrO_2 additive on the parameters of temperature dependence of initial permeability

Samples type	N 10^3	T_c (°C)	μ_{max}	T_m (°C)	β/α 10^3
No additive	1.79 ± 0.03	269.2 ± 0.3	430.8	242.5	4.88
Add. 0.1%	2.34 ± 0.05	264.7 ± 0.3	374	232.9	6.22
Add. 0.25%	2.05 ± 0.06	265.6 ± 0.3	358.2	229.5	10.52
Add. 0.5%	1.34 ± 0.03	265.3 ± 0.2	230.2	240.8	22

Where N–demagnetization coefficient; μ_{max}–the maximum of temperature dependence of initial permeability; T_m–position of a peak of the temperature dependence of the initial permeability on the temperature scale; β/α–defect structure of ferrite ceramic samples

where g = 2 and r = 2–exponent of power in (3), (4) for the model of initial permeability by Smith and Wijn; m, n, f–exponent of power in (5), (6); K_1–crystallographic magnetic anisotropy; γ_s–magnetostriction constant; α–average elastic stresses; N–demagnetizing factor; M_s–saturation magnetization; T_c–Curie point.

From the data in Table 2, it follows that with an increase in the ZrO_2 concentration up to 0.5 wt.% defect structure β/α of ferrite ceramics increased by 350%. At the same, the maximum of the temperature dependence of μ_i dropped by 45%. The other parameters do not change significantly with an increase in the ZrO_2 additive concentration.

As it can be seen from Table 2, the T_m first falls with an increase in the ZrO_2 concentration up to 0.25 wt.% (shift from the Curie point), and then sharply increases (shifts to the Curie point) with an increase in the ZrO_2 concentration to 0.5 wt.%. In addition, the demagnetizing factor does not increase monotonically with an increase in the ZrO_2 concentration but passes through a maximum at a ZrO_2 concentration of 0.1 wt.%.

Table 3 shows the comparative effect of ZrO_2 and Al_2O_3 additives on the μ_{max}, T_m and the parameters of the temperature dependence of the initial permeability [10].

Compared to the results of the Al_2O_3 adding to LiTiZn ferrite, the ZrO_2 addition also causes a similar increase in the defect structure β/α and a reduction of μ_{max}, but the character of the change in μ_{max} and the position of the peak on the temperature scale T_m is different.

From Table 3 it follows that with an increase in the concentration of diamagnetic additives Al_2O_3, the T_m parameter monotonically decreases, whereas with an increase in the concentration of ZrO_2, it passes through the minimum at 0.25 wt.%.

Table 3 The comparative effect of ZrO_2 and Al_2O_3 additives on the parameters of temperature dependence of initial permeability

Samples type	N 10^3	T_m (°C)	μ_{max}	β/α 10^3
No additive	1.79 ± 0.03	242.5	430.7	4.9
Add. 0.1% ZrO_2	2.34 ± 0.05	232.9	374	6.22
Add. 0.1% Al_2O_3	1.96 ± 0.04	237.9	400.3	8.9
Add. 0.25% ZrO_2	2.05 ± 0.06	229.5	358.2	10.52
Add. 0.25% Al_2O_3	2.28 ± 0.06	236.6	325	18.8
Add. 0.5% ZrO_2	1.34 ± 0.03	240.8	230.2	22
Add. 0.5% Al_2O_3	2.65 ± 0.05	226	299.6	28.9

In addition, the demagnetizing factor N increases with an increase in the concentration of Al_2O_3, which is not observed for the addition of ZrO_2.

In the case of both types of additives, a similar decrease in μ_{max} with an increase in the concentration of diamagnetic additives is observed. However, μ_{max} is less in the case of the ZrO_2 additive compared to the Al_2O_3 additive for each concentration (Table 3). Indeed, such behavior is connected with different ratios of additives in the grain volume and grain boundary for LiTiZn ferrite ceramics with different additives. It is possible that some part of the Al_2O_3 additive is introduced into the grain boundary as ZrO_2 into the volume of ferrite ceramic grains. As a result of this process, the concentration of ZrO_2 additive in the volume of ferrite ceramic grains is higher compared to samples with the use of Al_2O_3 addition. Consequently, the ZrO_2 addition is characterized by a greater influence on the domain wall motion in the grain volume, as well as on the initial magnetic permeability, including μ_{max}.

Figure 4 shows that the concentration of ZrO_2 affects the character of changes in the experimental temperature dependence of the initial permeability. With an increase in the concentration of ZrO_2 up to 0.25 wt.%, a shift of the maximum of this dependence

to the Curie point is observed. However, with an increase in the ZrO_2 concentration to 0.5 wt.%, the maximum shifts to the Curie point. Underline, that in the case of Al_2O_3 adding, a different character of the temperature dependence transformation is observed, at which the maximum with an increase in concentration to 0.5 wt.% shifts monotonically from the Curie point (Table 3).

In [11] for NiCuZn ferrites, a decrease in the maximum of the μ_i temperature dependence with an increase in the concentration of Al_2O_3 was found. The authors attribute this behavior to the influence of additives on the domain wall motion. Consequently, the impact of ZrO_2 additive on the temperature dependence of the initial permeability of LiTiZn ferrite ceramics shown above can be described by the same mechanism.

Thus, the μ_{max} parameter of temperature dependence of the initial permeability can be used to estimate the defect structure ore diamagnetic impurities in ferrite ceramics.

3.4 Magnetic analysis

Figure 5 shows the impact of diamagnetic ZrO_2 addition on the magnetic hysteresis loop parameters (Table 4). The magnetizing field is selected based on the saturation of the dependence of the maximum induction on the magnetic field strength $B_m(H)$. The introduction of ZrO_2 affects the residual induction B_r, the maximum induction B_m and the coercive force H_c.

It follows from Table 3 that B_r and B_s decrease monotonically, while H_c increases with increasing concentration of ZrO_2. Clearly, this behavior is due to the appearance and growth of demagnetizing fields associated with the action of elastic stress fields [5, 12–14]. Emphasize, with an increase in ZrO_2 to 0.5%, H_c increases by 50%.

3.5 The true physical broadening

The true physical broadening δ was determined for the same samples. The widths of the diffraction peaks from the (400) and (800) planes were determined, considering the doublet spectral line by the method of decomposition into Gaussian components [7].

According to the data in Table 5, with an increase in the concentration of ZrO_2 to 0.5%, the true physical broadening increases by 20%. A similar behavior is observed for the (800) diffraction peak.

Comparing the data in Table 2 with the data in Tables 4 and 5, it follows that H_c increases by 50%, and the true physical broadening δ—by 20% only, while the concentration of ZrO_2 increases to 0.5%. At the same time, the defect structure β/α, determined from the temperature dependence of μ_i increases by 350%. Consequently, our earlier proposed method for determining the defect structure with mathematical analysis of the temperature dependencies of μ_i significantly exceeds the sensitivity of typical magnetic and X-ray methods [7].

The obtained results showed that the ZrO_2 diamagnetic addition degrades some magnetic parameters of model samples of LiTiZn ferrite. Such behavior is typical for magnetic dilution of ferrimagnetic materials [5].

3.6 The defect structure and elastic stress

The width of the diffraction peaks is determined, in turn, by the elastic stresses in the material [15]. In this regard, it is interesting to establish the relationship between elastic stresses in the material and the defect structure β/α. Figure 6 shows the dependence between the width of the (400) diffraction peak and the defect structure β/α for LiTiZn ferrite ceramic samples with the addition of ZrO_2. Figure 7 shows the dependence between the width of the (400) diffraction peak and the ZrO_2 additive concentration.

The appearance of elastic stress of ferrite connected with baking ZrO_2 oxide particles in the ferrite matrix grains and the difference in the thermal expansion coefficients, the lattice structure of both phases. In this case, the residual stresses can be estimated according to the scheme proposed in [16]. At low concentrations of inclusions, the overlap of the elastic stress fields can be neglected, and in this case, the volume of the sample that has experienced strain will be proportional to the amount of the additive. Such behavior is observed for the studied model ferrite ceramics samples (Fig. 6 and Fig. 7).

Surely, Fig. 6 and Fig. 7 show a close to linear relationship between the diffraction peak width and the defect structure β/α and ZrO_2 additive concentration. Consequently, this parameter β/α likewise can be used to characterize elastic stresses in ferrite ceramics [7]. As a result, it was shown that an increase in elastic stresses in LiTiZn ferrite ceramics

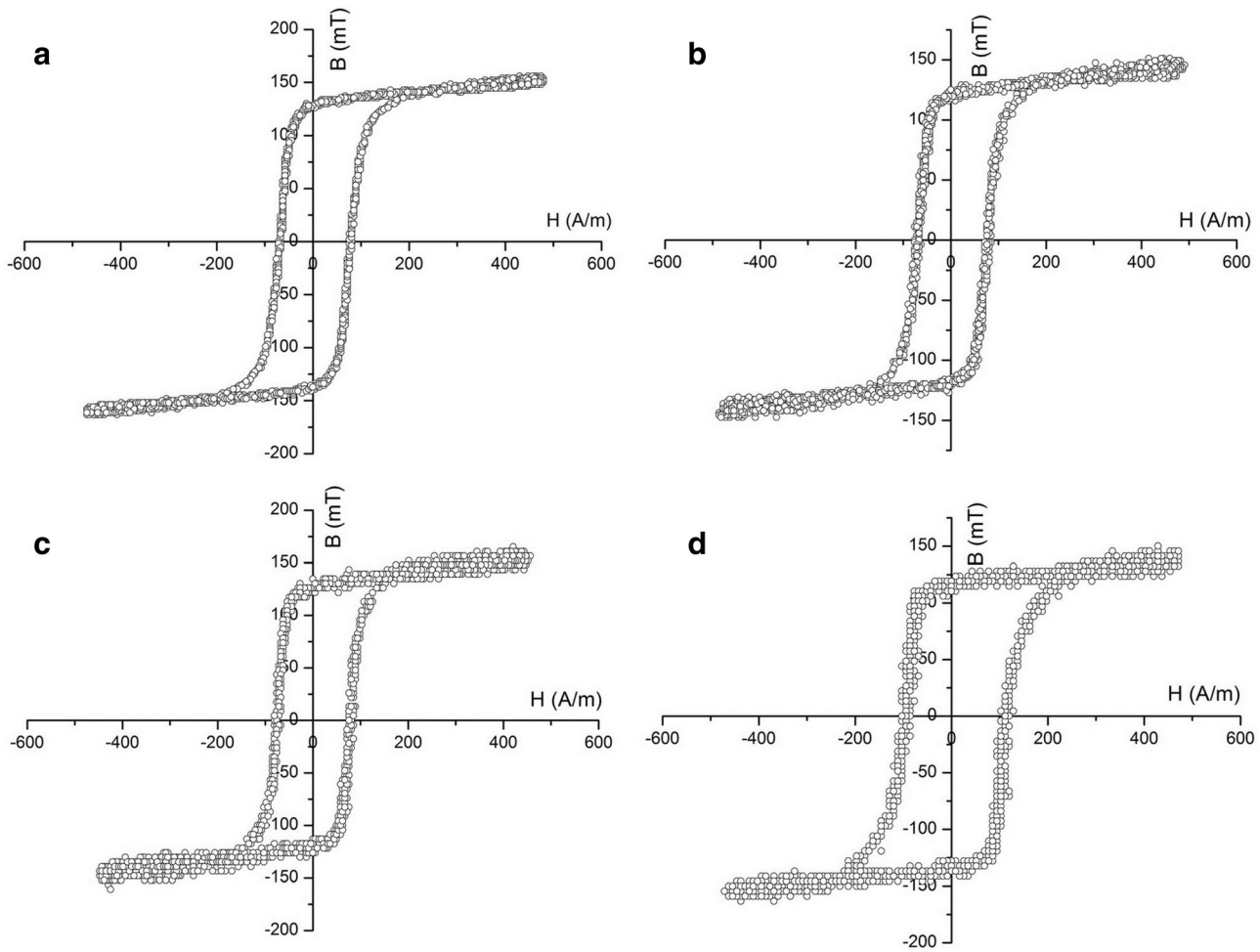

Fig. 5 Hysteresis loops for LiTiZn ferrite ceramic samples: **a** no additives; **b** 0.1% of ZrO_2; **c** 0.25% of ZrO_2; **d** 0.5% of ZrO_2

Table 4 Parameters of the hysteresis loop of LiTiZn ferrite ceramic samples with ZrO_2 additive

Samples type	B_s (mT)	B_r (mT)	H_c (A/m)
No additive	155.7	128.8	78.3
Add. 0.1%	145.6	121.6	79.8
Add. 0.25%	151	125	84.7
Add. 0.5%	143	120	119.6

Where B_r–residual induction; B_m–the maximum induction; H_c–the coercive force

Table 5 True physical broadening δ for reflex (400)

Samples type	W (degree)	δ (degree)
Standard	0.083	–
No additive	0.158	0.134
Add. 0.1%	0.163	0.14
Add. 0.25%	0.174	0.153
Add. 0.5%	0.181	0.161

Here W–peak width at half height

is caused by the introduction of diamagnetic ZrO_2 into the material. In this case, the elastic stresses of the model samples of ferrite ceramics are proportional to the defect structure β/α, determined from the temperature dependence of the initial permeability.

4 Conclusion

The previously proposed method for determining the defect structure of LiTiZn ferrite ceramic samples with ZrO_2 diamagnetic additive has been tested.

The high sensitivity of the method, in comparison with typical magnetic methods and XRD, was shown.

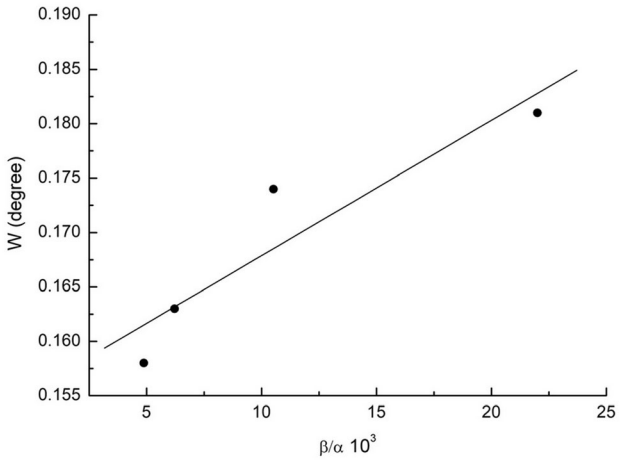

Fig. 6 Dependence of the (400) diffraction peak width on the defect structure β/α of model samples. Solid line—the approximation straight line

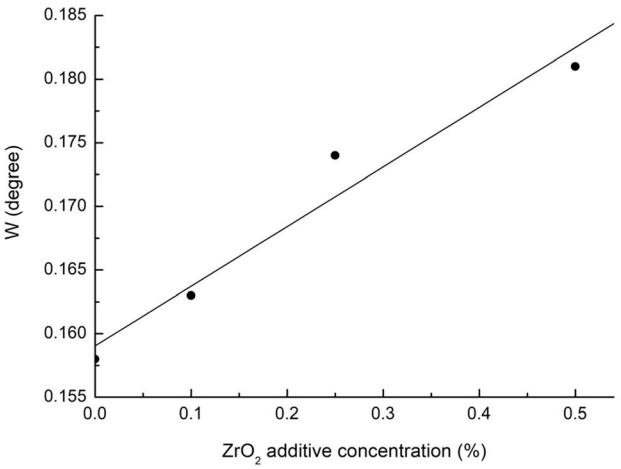

Fig. 7 Dependence of the (400) diffraction peak width on the ZrO_2 additive concentration of model samples. Solid line—the approximation straight line

Even the initial concentrations of the ZrO_2 diamagnetic additive (0.1–0.5 wt.%) affect the parameters of temperature dependency of initial permeability and the calculated defect structure.

It is shown that the defect structure of ferrite ceramics can be estimated from the maximum of this temperature dependence of the initial permeability near the Curie point.

It has been experimentally established that the defect structure is associated with the elastic stress of ferrite ceramics.

The results of this study display the possibility of nonmagnetic impurity monitoring in soft ferrite ceramics. Thus, the method is recommended for defect and impurity monitoring of soft ferrite ceramics and ferrite products.

Acknowledgements

The research is funded by The Ministry of Science and Higher Education of the Russian Federation in part of the science program (project FSWW-2020-0014). The experimental calculations are carried out at Tomsk Polytechnic University within the framework of Tomsk Polytechnic University Competitiveness Enhancement Program grant.

Declarations

Conflict of interest The authors declare that they have no known competing financial interests or personal relationships that could have appeared to influence the work reported in this paper.

References

1. P.P. Mohapatra, P. Dobbidi, J. Magn. Magn. Mater. **500**, 166354 (2020). https://doi.org/10.1016/j.jmmm.2019.166354
2. J. Li, D. Zhou, J. Alloys Comp. **785**, 13–18 (2019). https://doi.org/10.1016/j.jallcom.2019.01.148
3. P.P. Mohapatra, S. Pattipaka, P. Dobbidi, Ceramics Int. **45**, 25010–25019 (2019). https://doi.org/10.1016/j.ceramint.2019.04.040
4. Y. Guo, J. Zhu, H. Li, J. Mater. Sci. (2021). https://doi.org/10.1007/s10854-021-05419-2
5. J. Smith, H.P.J. Wijn, *Ferrites: Physical Properties of Ferromagnetic Oxides in Relation to Their Technical Application* (Phillips Technical Library, Eindhoven, 1959), p. 233
6. T. Zheng, J. Wu, Scripta Mater. **187**, 418–423 (2020). https://doi.org/10.1016/j.scriptamat.2020.06.063
7. A.V. Malyshev, A.B. Petrova, A.N. Sokolovskiy, A.P. Surzhikov, J. Magn. Magn. Mater. **456**, 186–193 (2018). https://doi.org/10.1016/j.jmmm.2018.02.032
8. P.K. Gallagher, J. Therm. Anal. Calorim. **49**, 33–44 (1997). https://doi.org/10.1007/BF01987419
9. G.K. Williamson, W.M. Hall, Acta. Metall. **1**, 22–31 (1953)
10. A.V. Malyshev, A.B. Petrova, A.P. Surzhikov, Ceramics Int. **44**, 20749–20754 (2018). https://doi.org/10.1016/j.ceramint.2018.08.073
11. S. Takane, H. Umeda, T. Aoki, T. Murase, Key Eng. Mater. **485**, 225–228 (2011)
12. W. Wang, R. Sun, S. He et al., 2D Mater. **8**, 015027 (2021). https://doi.org/10.1088/2053-1583/abc5cf

13. T. Zhang, Y. Wang, H. Li et al., ACS Nano. **13**, 11353–11362 (2019). https://doi.org/10.1021/acsnano.9b04726
14. Z. Xie, S. Lin, Z. Wang, Ceramics Int. **44**, 15912–15917 (2018). https://doi.org/10.1016/j.ceramint.2018.06.008
15. R.E. Dinnebier, S.J.L. Billinge, *Powder Diffraction: Theory and Practice* (The Royal Society of Chemistry, Cambridge, 2008), pp. 51–68. https://doi.org/10.1107/S010876730802850X
16. J. Selsig, J. Amer. Ceram. Soc. **44**, 419–422 (1961)